Composites Part B 148 (2018) 68–80

Contents lists available at ScienceDirect

Composites Part B

journal homepage: www.elsevier.com/locate/compositesb

Study on mechanical and ballistic performances of boron carbide reinforced Al 6061 aluminum alloy produced by powder metallurgy

Halil Karakoç[a,*], Şener Karabulut[a], Ramazan Çıtak[b]

[a] Department of Mechanical Engineering, Hacettepe University, 06935 Ankara, Turkey
[b] Department of Metallurgy and Materials Engineering, Gazi University, 06500 Ankara, Turkey

ARTICLE INFO

Keywords:
Metal-matrix composites (MMCs)
Mechanical properties
Impact behavior
Ballistic impact

ABSTRACT

In this study, the density, hardness, impact toughness, transverse rupture strength, tensile strength and ballistic resistance of Al 6061 alloy reinforced with boron carbide (B_4C) powders were studied to elucidate the influence of the ceramic content and production process on the physical and ballistic properties of the resulting composites. Powder-metallurgy and hot-extrusion techniques were used to manufacture the Al 6061-based metal matrix composites reinforced with 5 wt%, 10 wt%, 15 wt% and 20 wt% B_4C. The hot-rolling process was performed on a group of specimens to examine the effect on the mechanical and ballistic behaviors. The results revealed that a uniform particle distribution was achieved in a matrix structure and higher relative density values were measured in all specimens. The hardness, transverse rupture strength and tensile strength were improved and impact toughness was decreased with increasing volume fraction of B_4C particle reinforcement for both hot-extruded and hot-rolled specimens. The highest flexural strength was measured in hot-extruded specimens and the maximum tensile strength was obtained in hot-rolled composites. The deformation tests showed that transgranular cracking occurred on B_4C particles and particles were retained in the matrix. The hot-extruded, hot-rolled and laminated with two hot-rolled specimens were subjected to a ballistic test with a 7.62 mm × 51 mm M80 projectile for Type III and the ballistic resistance investigated by analyzing the hole surface in the armor. The hot-rolled and hot-extruded specimens were perforated in ballistic tests and exhibited ductile behavior with the petal failure mechanism. The two-layer hot-rolled specimens successfully absorbed the impact energy of the bullet with the lowest depth of penetration and smooth bulging.

1. Introduction

Aluminum (Al) has been the second most common metal, after steel iron material, used the most in our era for its good mechanical properties. Al and its alloys have an important place among engineering materials due to their low density, good heat and electric conductivity, resistance to corrosion and enhanced endurance. Al alloys have recently managed to take part especially in automobile, maritime and aviation industries and also in the defense industry with enhanced endurance and impact resistance properties. B_4C is one of the most important reinforcement materials for aluminum-based metal-matrix composites (MMCs) due to the excellent mechanical, physical and ballistic properties, with low density, high hardness and melting point [1–4]. Ibrahim et al. [5] fabricated pure aluminum and 6063 alloy-based MMC materials with reinforced B_4C using a powder-injection technique and investigated the impact toughness. Pure aluminum-based samples presented high toughness resistance compared with the aluminum 6063 alloy-based composites. The authors reported that the addition of Zr/Ti/Sc enhanced the particle/matrix adhesion. Another study by Ibrahim et al. [3] examined the fracture and mechanical properties of aluminum-based MMC reinforced with B_4C. Test samples were quenched in warm water and aged in the range of 25–400 °C for 10 h. The authors found that the homogeneous particle distribution in the matrix with strong bonding and maximum tensile strength was observed with Al 6063-based composites due to the precipitation of the Mg_2Si phase. They also reported that the B_4C particles were retained in the matrix after the deformation tests due to the presence of Ti. Karabulut et al. [1] studied the influence of B_4C reinforcement on tensile strength, transverse rupture strength (TRS), fracture and impact toughness of the aluminum 6061-based MMCs. They found that the tensile strength and hardness were increased while fracture toughness decreased with increasing weight fraction of particle reinforcement. In another study by Karabulut et al. [2] on the mechanical properties of aluminum alloy 7039 reinforced with Al_2O_3, B_4C and SiC, they found that AA7039/10 wt% Al_2O_3 composite specimens presented better mechanical behavior among the studied specimens. Karamış et al. [6] studied the

* Corresponding author.
E-mail address: halil.karakoc@hacettepe.edu.tr (H. Karakoç).

https://doi.org/10.1016/j.compositesb.2018.04.043
Received 8 May 2017; Received in revised form 9 March 2018; Accepted 20 April 2018
Available online 22 April 2018
1359-8368/

wear and failure mechanism of AA5083-and AA6063-based samples reinforced with 45, 30 and 15 wt% of SiC particle MMCs after high-velocity impact. Abrasion and melt–wear mechanism were observed on the deformed surface of the armor and plastic deformation was seen on the projectile nose. In a further study, Karamış et al. [7] investigated the failure mechanisms of AA5083 under ballistic impact against 7.62 mm and 9 mm projectiles. They reported that melted and solidified regions were observed at the hole surface due to the high friction. Karamış et al. [8] produced Al 7075 reinforced with Al_2O_3 using a squeeze-casting method and subjected to ballistic tests. They investigated the surface characteristics of the projectile after ballistic experiments. They found that the matrix material was melted and transferred to the projectile and breaks and plastic deformation were observed on the projectile nose tip. In another study, Karamış et al. [9] manufactured the AA 2024 reinforced with Al_2O_3 laminar MMCs by squeeze-casting and hot-pressing methods. They investigated the ballistic performance of the specimens and failure mechanisms after ballistic impact was evaluated. The authors reported that petalling and bulging formations were observed at the entrance and exit sides of the hole. Deep craters were also seen on both sides of the hole of the laminated structures. Demir et al. [10] investigated the ballistic impact behavior of aluminum alloys 7075 and 5083. Ballistic test results indicated that the best ballistic performance was obtained with the Al 7075-T651 alloy. Holmen et al. [11] studied the influence of different heat treatments on the ballistic behavior of the aluminum alloy 6070. They stated that the strength was a more significant feature than ductility in ballistic impact under test alloy with the given experimental procedures. Mondal et al. [12] examined the influence of three different heat treatment processes on the ballistic and mechanical properties of aluminum alloy 7075. The authors concluded that the under-age and peak-age alloys exhibited better ballistic resistance than the over-age alloy. Morphology and microstructural analyses of Al 2024/B_4C composites impacted by a 7.62 mm armor-piercing (AP) projectile were performed by Zhou et al. [13]. The authors reported three kinds of failure morphology at the projectile crater and no interface debonding between the particle and matrix. Liu et al. [14] produced a three-layer sandwich construction armor and the ballistic behavior of each layer was experimentally investigated. They used Ti6Al4V, carbon fiber plate and aluminum alloy as the third layer and joined with the Ti6Al4V first layer and middle layer with constructing alumina ceramic materials. They obtained the strongest ballistic resistance from the sandwich structure when Ti6Al4V was used in the first layer. Wadley et al. [15] produced a series of hybrid sandwich structures by fitting alumina with triangular, trapezoidal or rectangular cross-sections into the voids of extruded Al 6061-T6 and subjected to the impact tests using hard steel spheres to determine the ballistic performance of the fabricated structures. They reported that significant ballistic performance was achieved from trapezoidal prisms and additional performance enhancements were obtained when the trapezoidal prisms were changed to rectangular prisms. Garcia-Avila et al. [16] manufactured composite metal foam using a powder-metallurgy technique and investigated the ballistic resistance of the composite foam armor system against the 7.62 mm × 51 mm M80 and 7.62 mm × 63 mm M2 AP projectiles. They reported that the developed composite foam armor successfully stopped the projectiles with a minimum depth of penetration and absorbed 60–70% of the total impact energy of the bullet. Close agreement was obtained between experimental and finite element analysis results. McWilliams et al. [17] characterized the mechanical properties and ballistic resistance of ceramic fiber reinforced Al-2%Cu MMC and compared it with the matrix alloy. The authors observed that the MMC materials presented a strong tensile and compressive strength and decreased the ballistic performance when the volume fraction of fiber was higher than 3%. Gilioli et al. [18] developed a predictive model using finite element methods to determine the ballistic resistance of the aluminium 6061-T6. Then, they compared the experimental ballistic results and numerical simulation of the projectile impact. Authors were observed that a very good correlation between predictive model and test results. In other study, Manes et al. [19] performed an experimental and numerical investigation on Al 6061 tubes and studied the effect of the ballistic impact of 7.62 mm × 51 mm soft-core ball projectiles. They reported that the numerical simulations were indicated have an acceptable ability to reproduce the residual velocity of the projectiles, failure modes and residual stress field of the impacted area. Lee et al. [20] performed a numerical study impact behavior of carbon reinforced Al 6061-T6 MMCs. They stated that the fiber volume fraction was enhanced the ballistic resistance of the composite specimen and the deformation failure was influenced by the impact velocity. The ballistic performance of functionally graded Al 6061 and SiC composite specimens were experimentally studied by Aydın and Apalak using 9 mm Parabellum bullets. They found that the linear composite specimens were indicated the best ballistic resistance [21]. Jang et al. [22] produced an armor laminated with ZnO nanowires and anodized aluminum oxide nanoholes using nanostructured interfacial adhesion. The drop–weight impact tests were performed to the specimens and investigated the influence of the nanostructured interfacial adhesion. Authors found that the test pieces bonded with nanostructured interfacial adhesion exhibited the better ballistic protection. Clayton [23] developed an anisotropic nonlinear crystal mechanics model using a Taylor averaging scheme to study the influence of microstructure on ballistic resistance of the Al–Cu–Mg–Ag alloy. Test results indicated that the performance of the numerical simulation could be enhanced by tailoring microstructures. Numerous researchers are also studied the ballistic behavior of fiber based polymer composites and developed a prediction model using numerical simulations in composites under ballistic impact [24–31].

Al 7075 and Al 5083 aluminum alloys are used in the defense industry because of their good ballistic performance, formability and weldability. Al 6061 alloys have excellent formability, weldability, extrusion ability as well as high rigidity and good corrosion resistance. However, they have lower ballistic performance than Al 7075 and Al 5083. The purpose of this study is to develop composite materials with good microstructural, mechanical properties and ballistic performance by adding B_4C ceramic particles to the Al 6061 matrix structure due to the good extrudability. For this purpose, Al 6061 reinforced with 0, 5, 10, 15 and 20 wt% B_4C composite materials were fabricated by the powder-metallurgy technique with the application of powder mixing, pressing, extrusion, rolling processes and performing T6 heat treatment. The effects of B_4C reinforcement amount and production processes on microstructural and mechanical properties were studied and then ballistic performances of the developed composite specimens were investigated with a 7.62 mm × 51 mm M80 caliber projectile.

2. Experimental procedures

2.1. Production route of experimental specimens

The experimental specimens were fabricated from high-purity Al 6061 powders reinforced with weight fractions of 5, 10, 15 and 20% B_4C particles using the powder-metallurgy and hot-extrusion technique. The average size of B_4C powders used in the compositions was 10 μm and the Al 6061 particles had a median size of 100 μm. Aluminum and reinforcement powders were weighed on a Sartorius weighing instrument with 0.0001 g readability precision and then separately blended. Al 6061 and B_4C powders were mixed uniformly one-by-one for 45 min to achieve a uniform particle distribution in the matrix structure using a three-dimensional Turbula shaker–mixer. The blended Al 6061 and B_4C powders were uniaxially compacted under 300 MPa pressure with a cold-pressing die. The compacted block samples were sintered in an open atmosphere at 550 °C for 1 h using a Protherm-type furnace. After the sintering process, the specimens were extruded using a preheated extrusion mold and thus the dimensions of the fabricated specimens were 285 × 86 × 24 mm^3. The surface of the specimens was machined

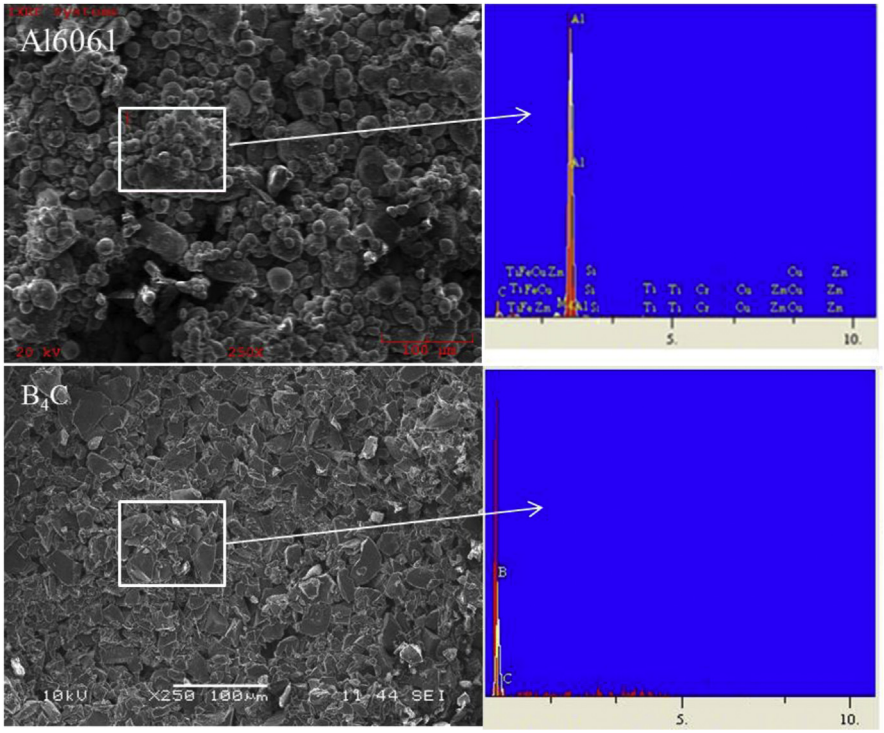

Elt.	Line	Intensity (c/s)	Error 2-sig	Conc	
Mg	Ka	2.40	0.980	0.826	Wt.%
Al	Ka	157.22	7.930	96.793	Wt.%
Si	Ka	1.16	0.681	0.739	Wt.%
Ti	Ka	0.99	0.628	0.562	Wt.%
Cr	Ka	0.69	0.524	0.461	Wt.%
Mn	Ka	0.81	0.568	0.619	Wt.%
Fe	Ka	0.00	0.000	0.000	Wt.%
Cu	Ka	0.00	0.000	0.000	Wt.%
Zn	Ka	0.00	0.000	0.000	Wt.%
			Total	100.000	Wt.%

kV	20.0
Takeoff Angle	35.0°
Elapsed Livetime	10.0

Elt.	Line	Intensity (c/s)	Error 2-sig	Conc	
B	Ka	13.87	2.354	83.102	Wt.%
C	Ka	0.39	0.393	16.898	Wt.%
			Total	100.000	Wt.%

kV	20.0
Takeoff Angle	35.0°
Elapsed Livetime	10.0

Fig. 1. SEM micrographs and EDS results for Al 6061 and B_4C powders used in the specimens.

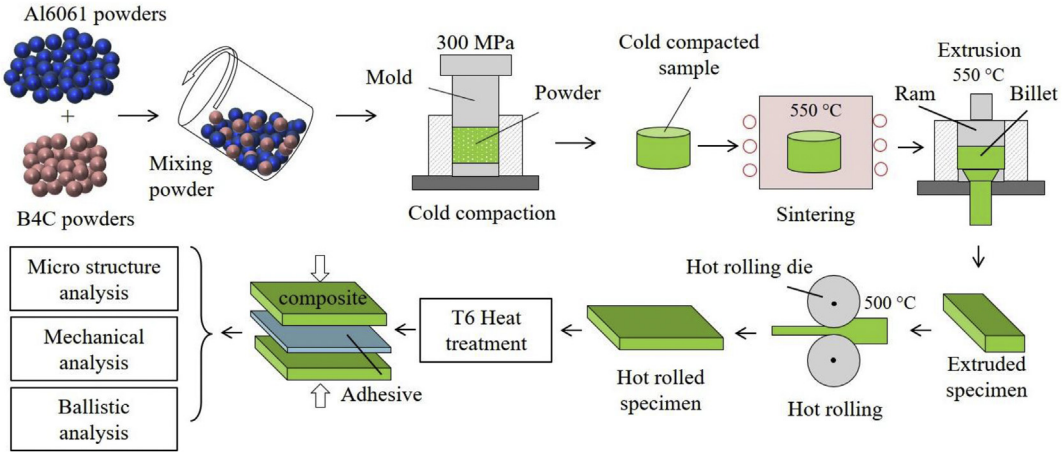

Fig. 2. Overview of the experimental process.

using a CNC milling machine to reduce the thickness to 20 mm and improve the surface quality of the specimens before the hot-rolling process. The specimens were subjected to a preheating process at 500 °C for 1 h, then to the hot-rolling process performed in three stages, keeping the specimens in the furnace at 500 °C for 30 min between each stage. Thus, the thickness of the specimens was 12.7 mm, solution heat treating was employed to increase the strength of hot-rolled composite plates at 530 °C for 1 h at a heating rate of 10 °C/min. Next, the composites were rapidly cooled in water to increase the hardness and aged at 175 °C for 8 h in a furnace. At the end of the production process, a group of hot rolled specimens were joined by using two components adhesive provided by sun-fix. These adhesives are very effective in bonding metals at room temperatures and can be mechanically processed. The compressive and tension strengths of the adhesive are around 80 MPa and 30 MPa, respectively. The scanning electron microscope (SEM) micrographs and energy dispersive spectroscopy (EDS) analysis results of Al 6061 and B_4C powders are given in Fig. 1 and the fabrication process of the specimens is presented in Fig. 2.

2.2. Mechanical and microstructural characterization

The physical and microstructural evaluations of composite specimens were evaluated by performing density, porosity, hardness, impact, bending and tensile strength measurements, microstructural and fractographic analysis. The densities of the specimens were determined using a Sartorius scale with a sensitivity of 0.1 mg according to the Archimedes principle and compared with the theoretical densities of Al 6061 (2.7 g/cm^3) and B_4C particles (2.4 g/cm^3). Theoretical densities of the composite specimens, ρ_{MMC}, were computed using eq. (1):

$$\rho_{MMC} = \rho_{Al} * V_{Al} + \rho_{B4C} * V_{B4C} \quad (1)$$

Where ρ_{MMC} is the density of the composites, V_{Al} and V_{B4C} are the volume fraction of aluminum and B_4C in matrix. A Zeiss Evo 50 SEM and a Leica DM4000M optical microscope were used for morphological characterization of the specimens under study. Hardness measurements were performed by applying a 2.5 mm ball tip and 31.25 kgf load for 5 s using an EMCO test duravision 200 hardness instrument. The hardness

measurements were performed at five different locations, and the mean value of hardness was computed for each specimens. The mechanical test specimens were cut to standard size with Mitsubishi CNC wire electrical discharge machining (WEDM). TRS and tensile strength tests were conducted using an Instron 3369 universal testing machine having a capacity of 50 kN. The tensile tests were carried out according to MPFI-10 [32] and MPFI-41 [33] at a constant strain rate of 1 mm/s. Impact tests were performed on a 150 J hammer energy capacity Instron Wolpert PW30 Charpy impact measurement machine to determine the impact energy of the samples. V-notched specimens were used for the impact measurements to study the impact energy of the specimens according to EN ISO 148.01.

2.3. Ballistic experiments

Ballistic experiments of the specimens were carried out using the guidelines included in the National Institute of Justice (NIJ) standard 0101.06 [34] for Type III threats. During the tests, the composite specimens with an average size of 80 mm × 120 mm were fixed on the movable target holder. Armour samples were placed between two pieces of plates and fixed with bolts from the four edges. The distance between the gun and target was 10 m and a G3 rifle and 7.62 mm × 51 mm M80-type projectiles were used in the tests. A group of preliminary ballistic tests were performed to determine the behavior of the specimens under study and impact velocity of the projectile. The impact velocities of the projectiles were measured in between 822 m/s and 838 m/s in preliminary and experimental ballistic tests. Several studies have been performed on the impact velocity and residual velocity of the projectile to determine the energy absorption of the armor [35,36]. In this study, the impact velocities of the projectiles were measured during the test, specific ballistic energy was calculated using the ballistic limit velocity and areal density values of the specimens. Three different group samples produced with hot-extruded, hot-rolled and laminated with two hot-rolled specimens were subjected to the ballistic experiments at 830 ± 8 m/s. Detailed specification of the specimens is presented in Table 1.

2.4. Experimental results and discussion

2.4.1. Mechanical and microstructural properties

Aluminum 6061-based MMCs reinforced with different weight fractions of B_4C were manufactured by powder metallurgy and the hot-extrusion method. A group of samples was subjected to a hot-rolling process to examine the behavior of the rolled specimens in terms of microstructure, mechanical properties and ballistic performance. Density and strength are significant criteria in the choice of a material for an engineering application and these two properties are often relevant to each other. The ratio of the tensile strength of the material and the density is useful for making comparisons of materials in automobiles and the aircraft industry in terms of energy and weight [37]. For this purpose, density, porosity, impact toughness, TRS, hardness measurements and fractographic evaluations were performed. The influences of the microstructural and physical properties on the ballistic performances were investigated. Density and porosity measurements were made at each stage of the production of the composite specimens before sintering, after sintering, extrusion and hot-rolling processes. The porosities of the specimens were calculated by the difference between the calculated and measured densities of each composite. The theoretical densities were also calculated depending on the weight fraction of the reinforcement and matrix. The lowest density was observed in the cold compact samples due to being not yet fully processed before sintering, as expected. The highest densities were obtained after the hot-extrusion and rolling processes. The density of the specimens decreased with increasing the weight fraction of B_4C reinforcement as expected due to the lower density of B_4C particles compared to Al 6061. This can be also attributed to increased porosity rate depending on the increasing weight fraction of the B_4C reinforcement in the matrix (Fig. 3), as reported in previous studies [38]. As can be seen in Fig. 3, more porosity was observed at higher particle reinforcements due to the increase in surface area of B_4C reinforcement particles and agglomeration. It has been observed that the hot-extrusion process has a considerable influence on the density change. The relative density in Al 6061 alloy without reinforcement increased to over 99%, while the relative density at 20% B_4C was 99.97%. The hot-rolling process did not significantly affect the density but reduced the porosity of the specimens. However, it was observed that density values of hot-rolled specimens increased at a very low rate according to the hot-extruded specimens due to the reducing pore space between the particles with applied pressure. The relative densities of all samples regardless of B_4C reinforcement ratio were obtained above 98%, as in the extrusion process (Fig. 3).

The SEM micrographs were taken to evaluate the particle distributions in the matrix structure and interface bonding between the matrix and B_4C particles. B_4C powders are homogeneously dispersed in the matrix structure and minor agglomerations were seen in the matrix (Fig. 4). In general, acceptable interface bonding was achieved between the B_4C reinforcement powders and Al 6061 alloy in hot-extruded specimens. However, micro voids and failure modes were observed around the B_4C reinforcement particles in 15 and 20 wt% B_4C samples in hot-rolled specimens. The reinforcement particles approached each other with the increasing amount of the B_4C powders and excessive plastic deformation of the specimens during the hot-rolling process. These microstructural failures are noticeable in agglomerated regions in the matrix structure. As a result, this could produce microvoids, cracks and failure modes of the matrix material.

The comparative findings of mean hardness, TRS, tensile strength and fracture toughness of the hot-extruded and hot-rolled composite specimens are depicted in Fig. 5. The mean hardness of the specimens increases with increasing reinforcement amount of B_4C for both hot-extruded and rolled composites due to the higher Vickers hardness of B_4C. The highest hardness values are measured on the Al 6061 reinforced with 20 wt% B_4C. B_4C particles could be considered an important factor in increasing the stiffness of the composites by creating tension in the matrix structure. It was observed that the hardness values were higher in the hot-rolled samples than in the hot-extruded samples. This is because the hot-rolling process causes deformation hardening. The relative density changes and porosity ratios in the samples obtained after the extrusion and rolling processes have a significant effect on the change of hardness.

Table 1
Specifications of the composite specimens.

Specimen group	Target material	Production method	Thickness (mm)	Areal density (kg/m^2)
1.group	Al 6061	Hot rolling	12.7	34.163
	5% B_4C	Hot rolling	12.7	34.036
	10% B_4C	Hot rolling	12.7	33.909
	15% B_4C	Hot rolling	12.7	33.655
	20% B_4C	Hot rolling	12.7	33.274
2.group	Al 6061	Hot extrusion	25.4	68.072
	5% B_4C	Hot extrusion	25.4	67.818
	10% B_4C	Hot extrusion	25.4	67.564
	15% B_4C	Hot extrusion	25.4	66.802
	20% B_4C	Hot extrusion	25.4	66.294
3. group	10% B_4C + Al 6061	Laminated- hot rolled	25.4	68.072
	20% B_4C + Al 6061	Laminated- hot rolled	25.4	67.945
	10% B_4C + 5% B_4C	Laminated- hot rolled	25.4	67.691
	15% B_4C + 5% B_4C	Laminated- hot rolled	25.4	67.437

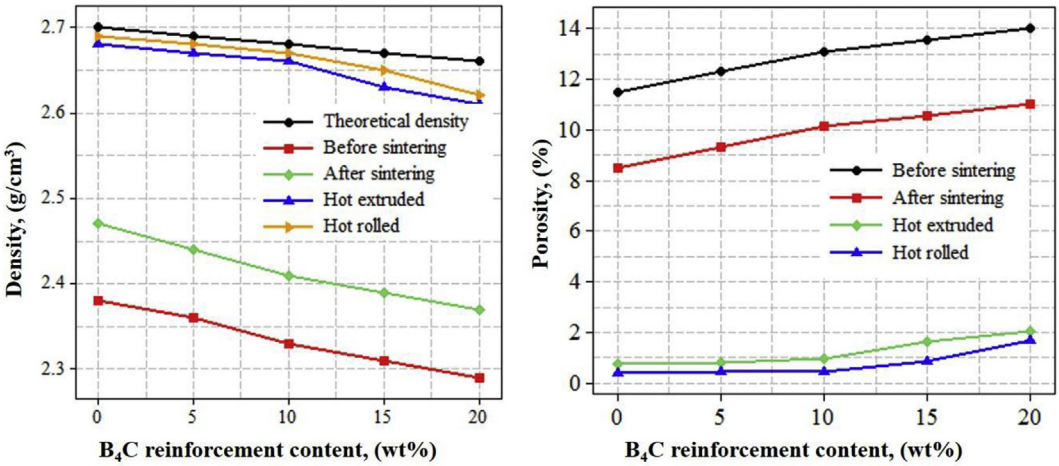

Fig. 3. Density and porosity measurements of the specimens.

The TRS measurements were conducted to determine the deformability and fracture behavior of the hot-extruded and rolled specimens with varying amounts of B_4C particles. The influence of B_4C reinforcement amount and production process on the three-point bending resistance of the specimens is depicted in Fig. 5. The three-point bending resistance of the hot-extruded specimens increased from 400 MPa to 650 MPa on increasing the B_4C particles but the TRS of the 20 wt% B_4C specimen was reduced to 400 MPa from 650 MPa at 15 wt %. The hot-rolled specimens generally exhibited ductile behavior under the three-point bending resistance tests and the specimens bent without breaking in the applied force direction. As a result of bending, the crack mechanism was initiated on the opposite side of the applied force direction of all composite samples. The crack mechanism was more prominently seen depending on the increasing reinforcement ratio of the B_4C particles. The highest TRS was achieved in 5 wt% B_4C specimens and decreased slightly from 562 MPa to 441 MPa with the rising amount of B_4C content.

The tensile strength of the hot-extruded unreinforced Al 6061 increased from 155 MPa to 180 and 190 MPa in the 5 wt% B_4C and 10 wt % B_4C reinforced-composite specimens, respectively. Then, the tensile strength decreased slightly to 170 and 150 MPa in the 15 wt% B_4C and 20 wt% B_4C reinforced-composite specimens, respectively, with increasing B_4C content in the matrix structure.

The tensile strength of the hot-rolled specimens was improved compared with the hot-extruded specimens. Maximum tensile strength of 210 MPa was measured in the 5 wt% B_4C reinforced-composite specimen and then decreased from 210 MPa to 170 MPa with increasing weight fraction of the B_4C content. The tensile strength of B_4C-reinforced hot-rolled specimens was remarkably enhanced compared with unreinforced Al 6061 alloy due to the decreasing porosity space between the matrix and reinforcement particles with applied rolling pressure. The lower tensile strength value of 170 MPa was obtained in the 10 wt% B_4C reinforced-composite specimen. The reason for the decreasing tensile strength value for 10 wt% B_4C-reinforced-composite specimen may be due to the agglomeration of the B_4C particles and voids between the matrix and B_4C particles as described in a previous study [1]. The tensile strength was improved by about 23% in hot-extruded 10 wt% B_4C and 35% in hot-rolled 5 wt% B_4C particle-reinforced

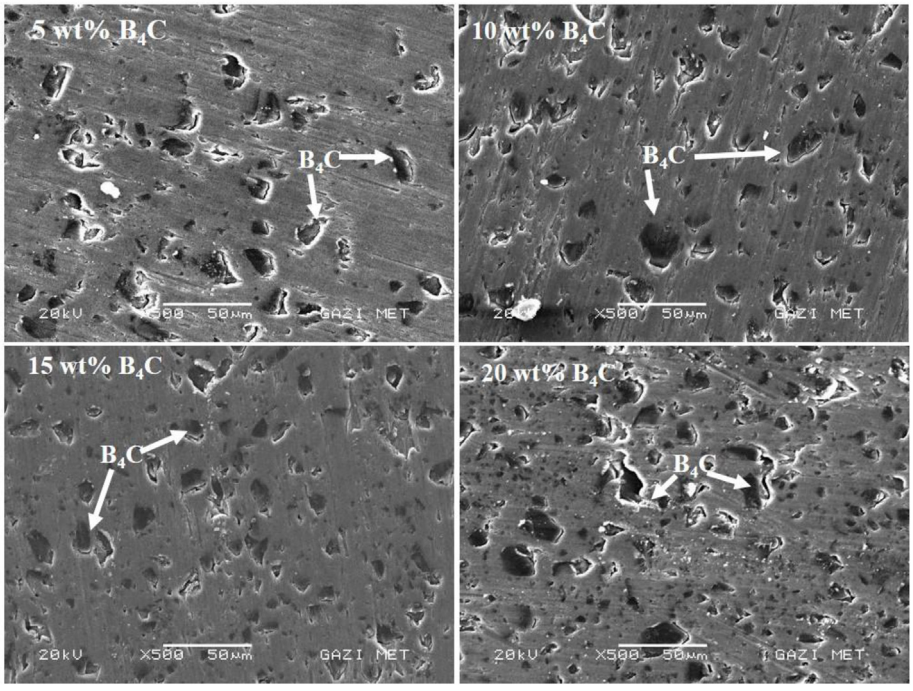

Fig. 4. B_4C particle distributions in the matrix structure.

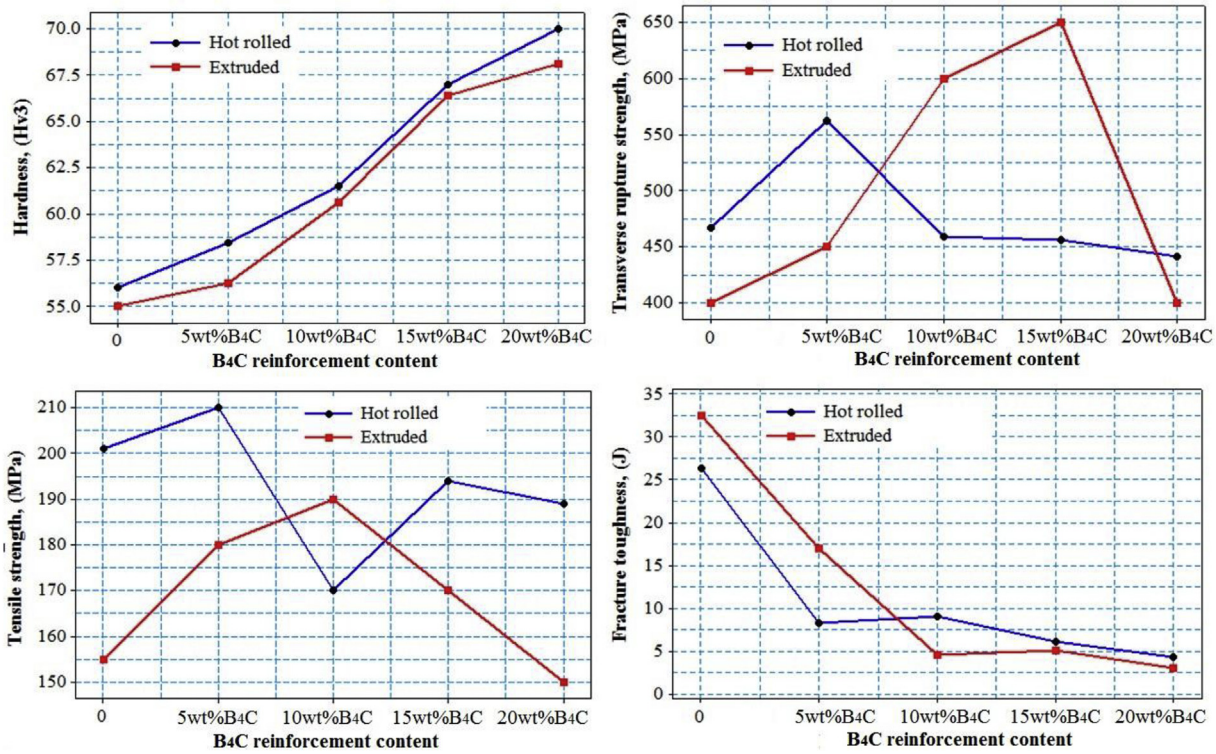

Fig. 5. Mechanical observations for the experimental specimens.

Al 6061 composite specimens compared with unreinforced hot-extruded Al 6061 aluminum. These enhancements can be explained by the transferring of tensile stress from the matrix to B_4C reinforcement particles improving the tensile strength of the samples [1,39]. Lower tensile strength and TRS values were measured in the case of Al 6061 reinforced with higher volume fraction of B_4C particles. These mechanical defects could be attributed to a number of possible factors, such as agglomeration, small holes and cavities in matrix and weak bonding between the particles and matrix structure [2]. Charpy impact tests were performed to determine the amount of energy absorbed by the composite specimens during fracture. The experimental results showed that the fracture toughness of hot-extruded and rolled specimens was decreased depending on the amount of the B_4C reinforcement content. As expected, the B_4C reinforcement reduced the ductility of the composite specimens. The maximum fracture toughness was measured in unreinforced hot-extruded Al 6061 alloy with 32.5 J, while the lowest impact energy was found in 20% B_4C reinforced-composite specimen with 3 J.

The fracture surfaces of both hot-extruded and rolled composite specimens were analyzed by SEM micrographs and EDS after the Charpy impact tests (Figs. 6 and 7). We observed that the B_4C particles are embedded in the matrix structure from the SEM and EDS analysis. Transgranular cracks occurred on the B_4C particles without debonding from the matrix. The remaining B_4C particles in the fractured surface after the impact test are evidence for the good interfacial bonding between the matrix and reinforcement particles. Thus, it can be assumed that the other side of the cracked B_4C particles retained the other part of the fractured surface. These embedded B_4C particles act as a crack stopper and prevent the rapid progression of cracks through the matrix structure. Thus, the deformation of the composites was limited, which improved the TRS of the specimens. However, some crack effects were seen on the fracture surfaces of the hot-rolled specimens due to the applied rolling pressure causing the forced motion of dislocations. The existence of large deep voids and small dimple shapes on the fractured surface show the good ductility of both hot-extruded and rolled composite specimens.

2.5. Ballistic properties

The ballistic performance of armor specimens produced by hot-extruded and hot-rolling methods was studied and the deformation behavior and failure mechanism of the composite specimens were analyzed under ballistic impact. Three different specimens were used in the ballistic tests and the effects of the production method and weight fraction of the B_4C reinforcement on the ballistic resistance were investigated. The composite armor was fastened to the target on the back plate and one ballistic shot was performed for every composite specimen to analyze the failure mechanism clearly. The specimens were cut carefully to an appropriate size using WEDM for microstructural evaluations after ballistic tests. Macro- and micrographs were taken of the entrance and exit points of the armor. Macro examinations of the hot-rolled armor can be seen in Fig. 8. All the hot-rolled composite specimens with a thickness of 12.7 mm were perforated by the projectile and specimens did not resist the impact of the projectile. Minor crack effects were seen on the front face of the unreinforced Al 6061 test specimen and material flow lines are observed in the direction of the projectile. Material accumulation and longitudinal cracks were formed in the center of the sample because of the thermal effect. Similar deformation mechanisms were also observed in the 5 wt% B_4C reinforced-composite specimen. Both specimens exhibited ductile behavior and relatively smooth surfaces were seen along the penetration zone. However, the spalling deformation occurred at the end of the hole in the 5 wt% B_4C reinforced-composite specimen. Radial cracks and spalling formations were increased in the front and back face of the 10–20 wt% B_4C reinforced-composite specimens depending on the increasing weight fraction of the B_4C reinforcement. The hole surface of the composite specimens was a bit rough due to the increasing friction between B_4C particles and the projectile surface. As shown in Fig. 8, the jacket of the projectile peeled and remained in the exit side of the hole for all experimental composite specimens under study due to the friction between the matrix surface and projectile. The remaining copper jacket of the projectile in the hole is significant for the ballistic resistance of the armor system because the peeled lead core can be easily

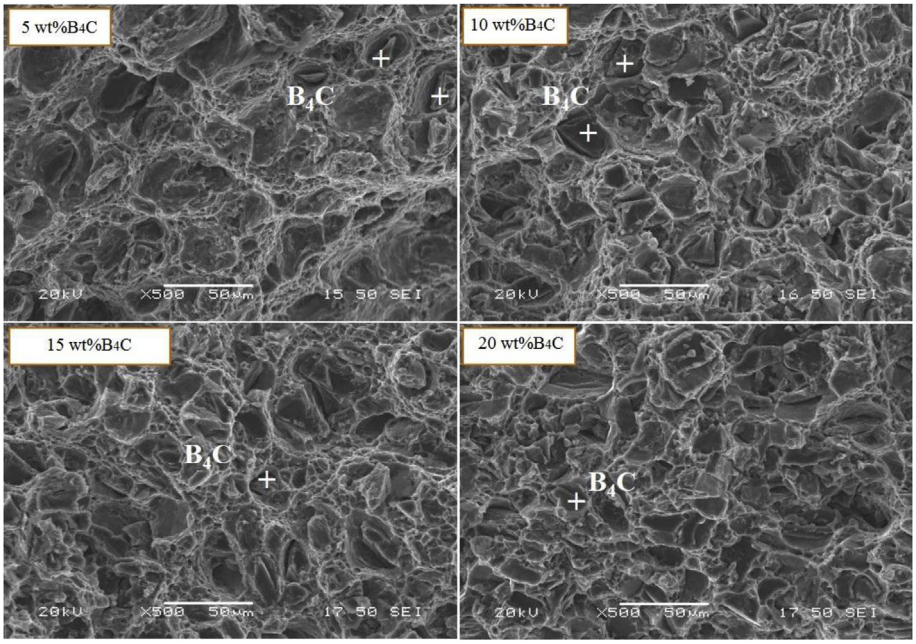

Fig. 6. Fracture surfaces for hot-extruded composite specimens.

wear and decreases the abrasive resistance of the projectile resulted in increasing the ballistic efficiency of the armor [8,40,41].

The hot-extruded composite specimens with a thickness of 25.4 mm were also perforated by the projectile, similar to hot-rolled armor, and presented a ductile behavior under ballistic tests (Fig. 9). Different petal formations were observed around the entry and exit of the hole depending on the weight fraction of the reinforcements in the matrix structure B_4C particle in unreinforced hot-extruded Al 6061, 5 and 10 wt% B_4C reinforced-composite specimens. Petal formation did not occur with 15 and 20 wt% B_4C reinforced-composite specimens and instead of this, detachments in the area surrounding the impact were observed at the rear surfaces of the composite armor. Macrocracks occurred at the end of the inside of the hole in the B_4C reinforced-composite specimens. These cracks progressed to the outside of the hole and some parts were separated from the specimens due to the reduced ductility in the composite specimens. Spalling failure formations are also observed at the back face of the armor specimens with the increasing amount of B_4C reinforcement. In addition, it was observed that the penetration channels have a different yaw impact angles (Figs. 8 and 9.) The angle between the entry and the exit hole was exhibited the different behavior depending on the weight fraction of the B_4C particles in matrix and fabrication method of the specimens. The small yaw angles were occurred in B_4C reinforced hot rolled composite specimens because of the isotropic nature of the stress field in hot rolled composite specimens. The specimens showed the same behavior due to the homogeneous internal structures and uniform particle distributions. Hence, the projectile was not indicated any preferential direction [42]. On the other hand, unreinforced hot rolled Al 6061 and hot extruded specimens showed the different ballistic behaviors and we observed larger yaw angles compared to hot rolled specimens. However, the yaw angles were decreased with increasing B_4C particle reinforcement and the variation in preferential direction of the bullet may be attributed to

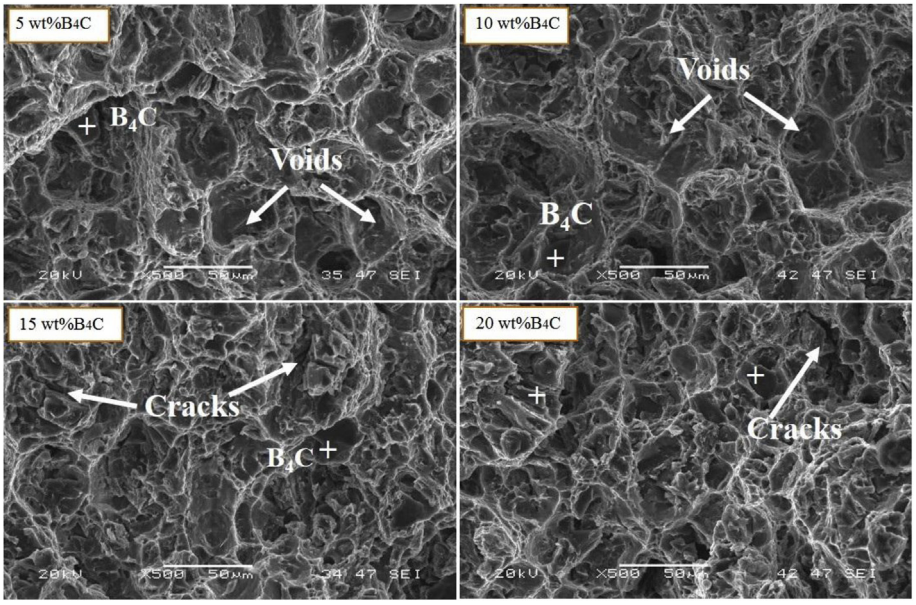

Fig. 7. Fracture surfaces of hot-rolled composite specimens.

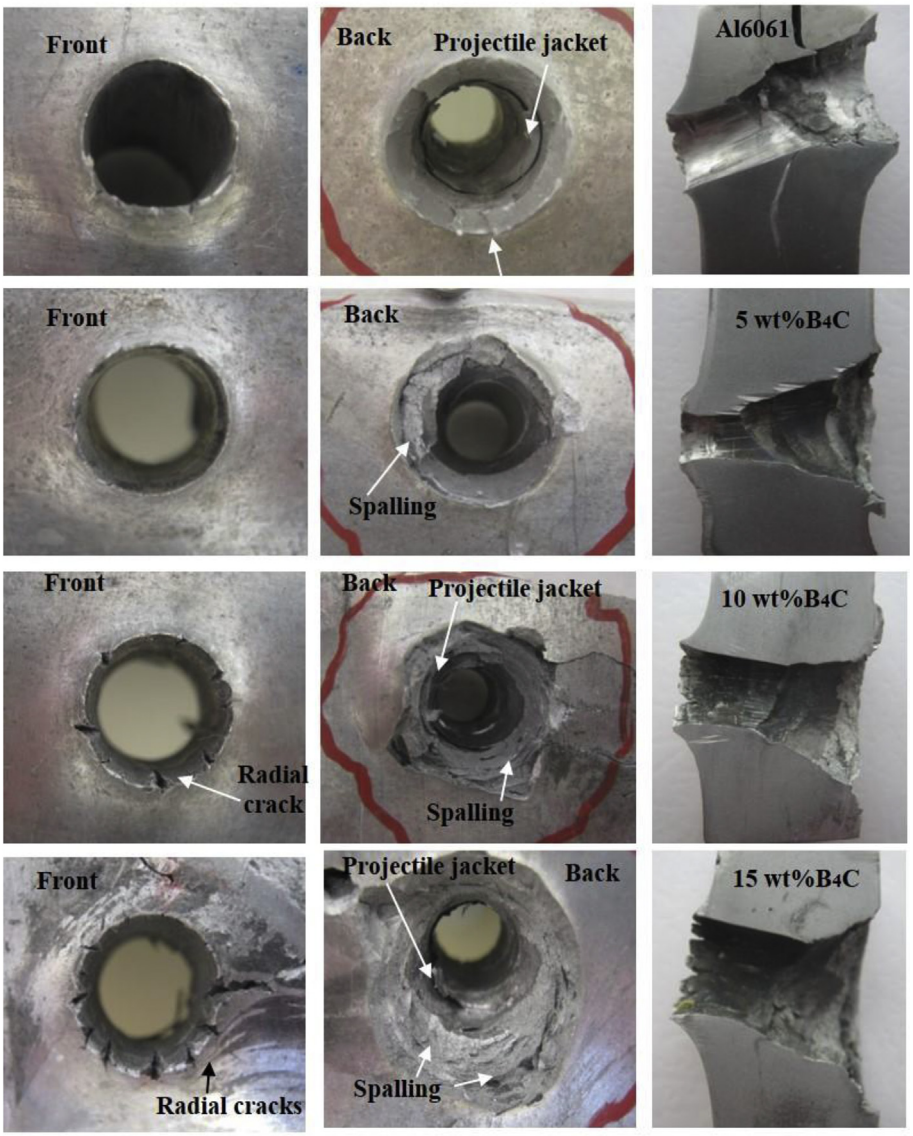

Fig. 8. Digital images and overview of the ballistic performances of the hot-rolled specimens.

the non-isotropic nature of the specimens (Fig. 9).

The copper jacket of the projectile was peeled and remained in the hole in hot-rolled specimens and evidence is presented in Fig. 8. Hence, it can be stated that the hot-rolled specimens exhibited more resistance than the hot-extruded specimens. Therefore, two different 12.7 mm thick hot-rolled specimens were joined to each other using metal-bonding adhesive and the ballistic performance of these two-layer specimens was investigated in the third stage of the ballistic tests. The sequence of the layers was determined depending on the experiences of the one layer ballistic shots and volume fraction of the B_4C particle reinforcement in matrix structure. Aluminum matrix material containing 10 wt%, 15 wt% and 20 wt% B_4C particulates was chosen as the main impact energy-absorbing layer. In addition, unreinforced Al6061 and 5 wt% B_4C reinforced MMC were determined as a backing plate due to the higher tensile strength and thus delays the action of the beginning the tensile failure and improves the ballistic performance of the armour. Hence, in the first layer of the armor, Al 6061 reinforced with 10 wt%, 15 wt% and 20 wt% B_4C specimens were used, and unreinforced Al 6061 and 5 wt% B_4C-reinforced-composite specimens were preferred in the second layer of the armor due to the ductile structures. Ballistic test results showed that the use of a ductile specimen as a second layer of the armor provides a stronger ballistic resistance and prevented some possible failure mechanisms. As can be seen in Figs. 10–13, two-layer specimens with 25.4 mm thickness absorbed the total kinetic energy of the bullet. The first layer of the armor was perforated and the second layer of the armor stopped the projectile with the minimum depth of penetration and deformation defined by NIJ standard. It was observed that the composite specimen containing B_4C particles in the first layer caused deformation of the projectile and the second layer of the armor successfully absorbed the kinetic energy of the bullet. To sum up, laminated specimens were exhibited a more ballistic resistance and this can be attributed that the projectile may be rebounded at the adhesive interface from one preferential direction of perforation channel to another perforation channel at the adhesive interface.

In the ballistic experiments of the 10 wt% B_4C and Al 6061 laminated specimens, minor crack formation at the entrance of the projectile and bulging formations on the rear face of the armor were seen (Fig. 10). Bulging formations were observed on the rear face of the armor. A small amount of radial cracking only occurred in the combination of 5 wt% and 15 wt% B_4C-composite specimens on the bulging formation having the highest penetration depth at the back face of the armor (Fig. 11). Using a ductile specimen as a backing layer of the armor increased the ballistic resistance of the specimen and decreased

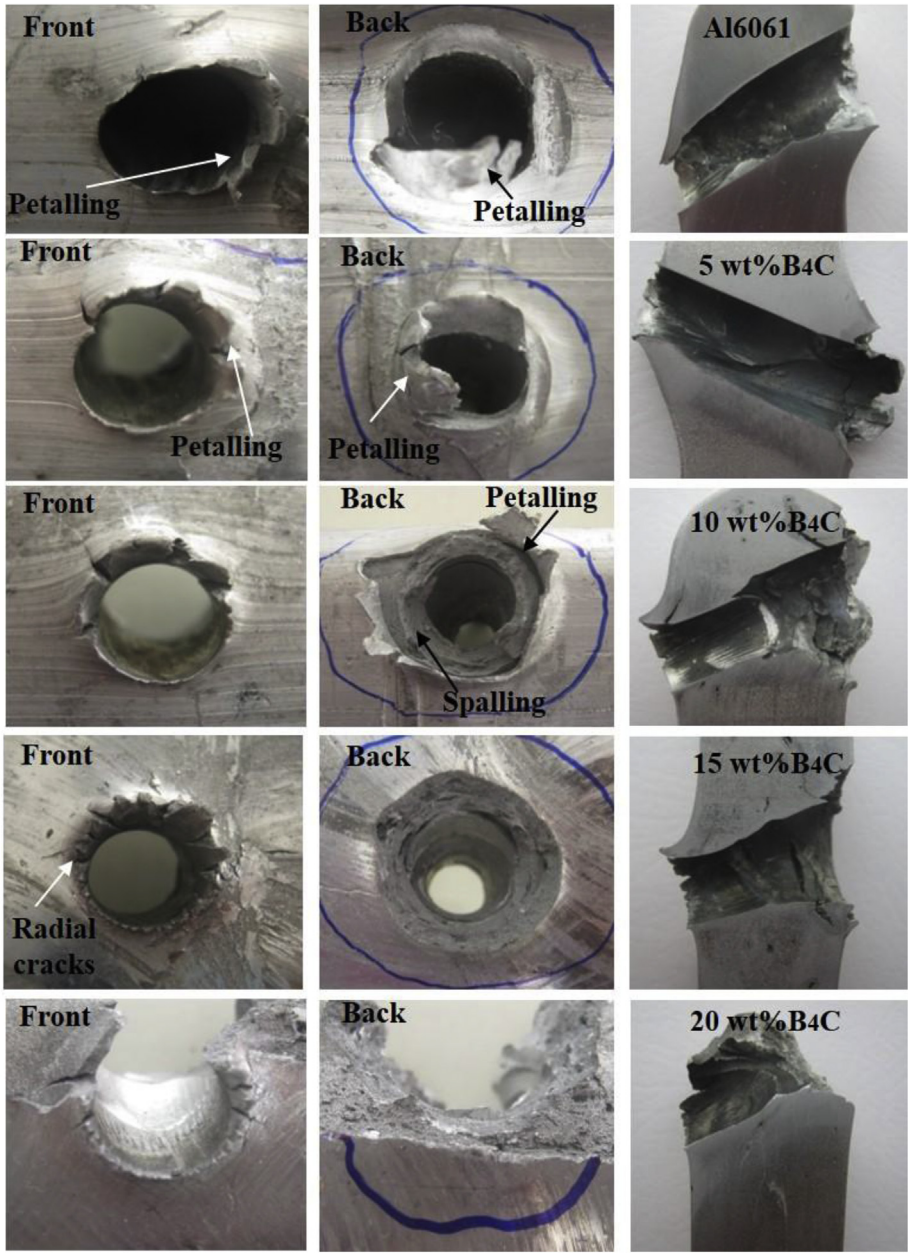

Fig. 9. Digital images and overview of the ballistic performances of the hot-extruded specimens.

the possible failures, such as spalling and cracks. Among the layered composite specimens, successful ballistic results were obtained in 5 wt % and 10 wt% B_4C composite specimens with the lowest depth of penetration. Fig. 11 presents SEM micrographs of the penetration area after projectile impact and it can be seen that the surface of the penetration zone was smooth and no failure mechanism was generated. The presence of some melted lead was found in the EDS analysis of the penetration area, as shown in Fig. 11. The presence of the lead demonstrates the transfer of lead at the back of the bullet core in the jacket from the projectile to the penetrated surface of the armor due to the frictional heating at the end of the hole [10].

Radial cracks were found in the entrance of the first layer and these cracks are increased in 15 wt% and 20 wt% B_4C particle-reinforced-composite specimens (Figs. 12 and 13). As shown in Fig. 11, the projectile first caused melting of the aluminum matrix and then the molten aluminum solidified on cooling. We can estimate from the molten aluminum clusters that a large amount of heat was generated in the penetration zone (Fig. 12). Similar observations were reported by Karamış [7,14].

In the entrance of 5 wt% and 15 wt% B_4C composite specimens, radial cracks around the hole were observed and bulge formation with a small number of cracks due to tensile stresses was seen on the rear face of the armor. It can be concluded that B_4C reinforcement particles in the matrix were not pulled and presented a good interface bonding between the matrix and reinforcement particle, as can be seen in the SEM micrographs in Fig. 13.

2.6. Specific ballistic energy of the specimens

The ballistic limit velocity and specific ballistic energy were used to elucidate the ballistic performance of the Al 6061 alloy reinforced with B_4C. Ballistic limit is the minimum velocity expected to full penetrate the armor and calculated the arithmetic mean value by using highest partial perforation and the lowest full perforation impact velocities. Hence, knowing the ballistic limit velocity (*BL*), it is possible to determine the specific ballistic energy of the bullet. The ballistic limit

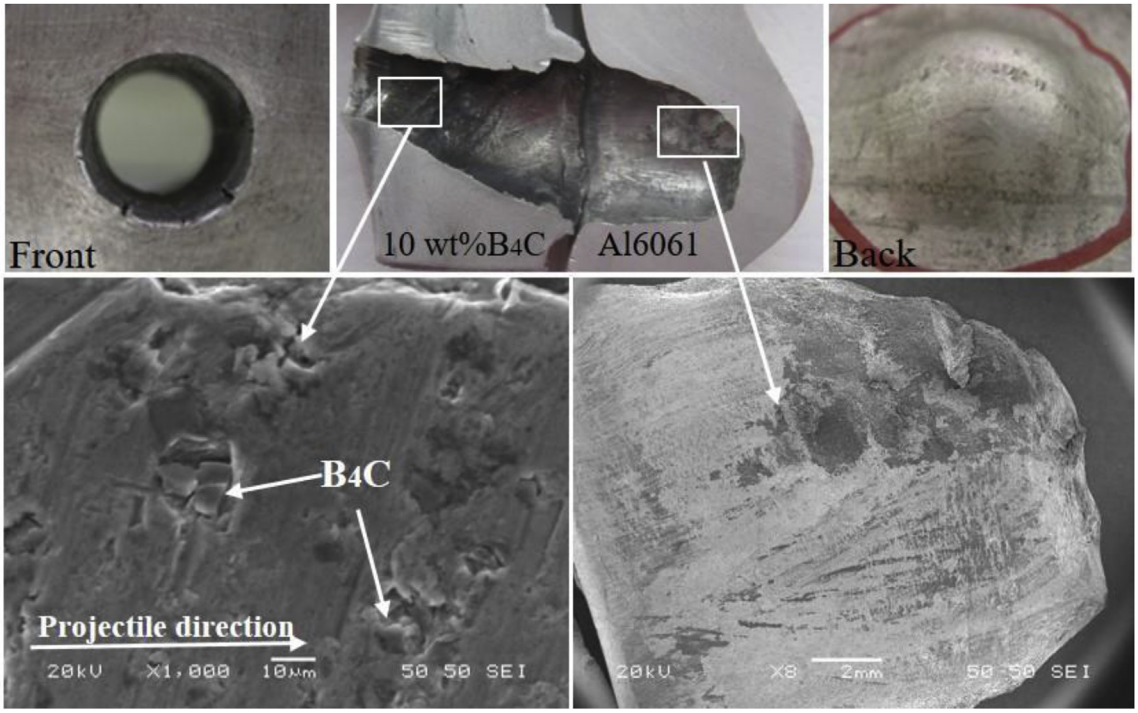

Fig. 10. Digital images of the front face, back face and cross sectioning of impacted armor. SEM analysis on the hole of 10 wt% B_4C and Al 6061 laminated armor.

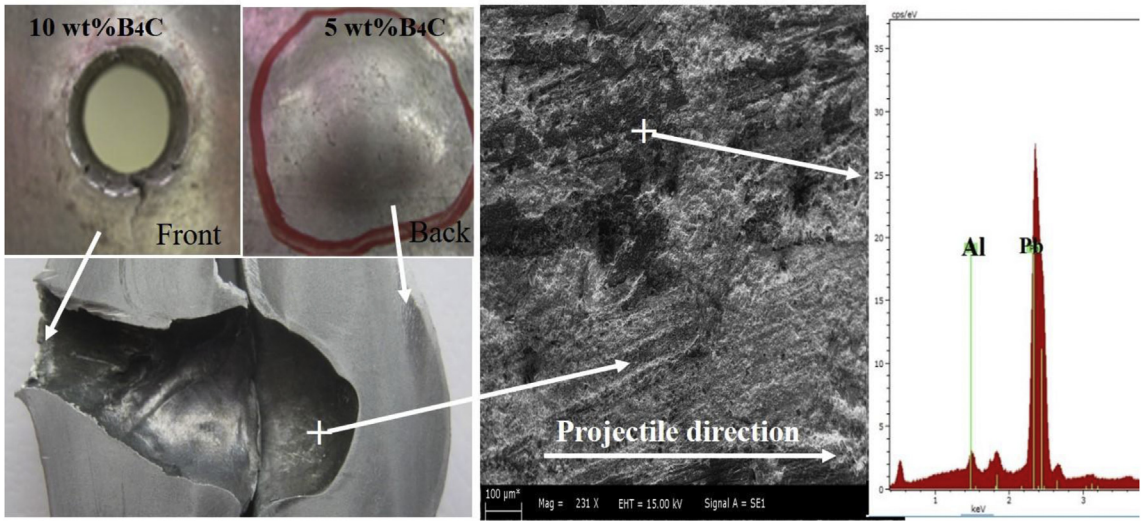

Fig. 11. Digital images of the front face, back face and cross sectioning of impacted armor. SEM and EDS analysis observations on the hole for 10 wt% and 5 wt% B_4C laminated composite specimens.

energy E_{BL} is a kinetic energy of the bullet and can be expressed in the following Equation (2).

$$E_{BL} = \frac{1}{2} m V_{BL}^2 \tag{2}$$

where m is the mass of the bullet in kilogram. Then, the ballistic limit energy of the bullet was divided by the areal density (ρ_A) of the specimens [43] to determine the specific ballistic energy of the armor using the following equation (3);

$$\textit{Specific ballistic energy } (Jm^2/kg) = \frac{E_{BL}}{\rho_A} \tag{3}$$

The areal densities of the specimens are presented in Table 1 and Fig. 14 depicts the variation curve of the specific ballistic energy of the specimens. The specific ballistic energy was improved with increasing volume fraction of B_4C particle reinforcement for all specimens under the study. It was noted that the laminated specimens had a higher specific ballistic energy depending on the armors thickness. However, the specific ballistic energies of the hot rolled specimens of 12.7 mm thickness are nearly equal to the specific ballistic energy of the laminated specimens. The extruded specimens was not exhibited a better performance with the thickness of 25.4 mm and the specific ballistic energy values were obtained in between 22.20 and 22.62 Jm^2/kg.

3. Conclusions

In this study, Al 6061 and 5 to 20 wt% B_4C particle-reinforced Al 6061 composite specimens were fabricated using the powder-metallurgy technique. Density, porosity, hardness, fracture toughness, fracture surface analysis, TRS and tensile strength of hot-extruded and

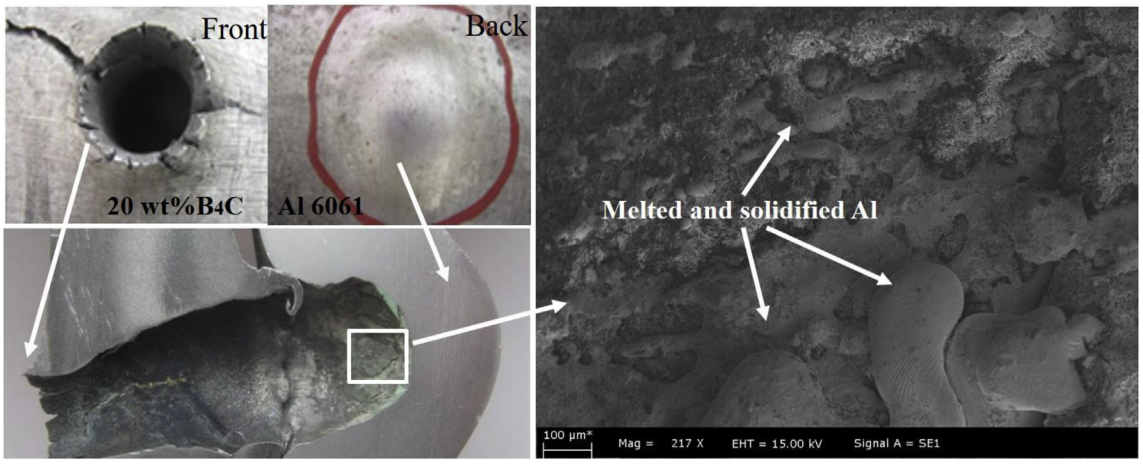

Fig. 12. Digital images of the front face, back face and cross sectioning of impacted armor. SEM images of the melted area at the end of the hole.

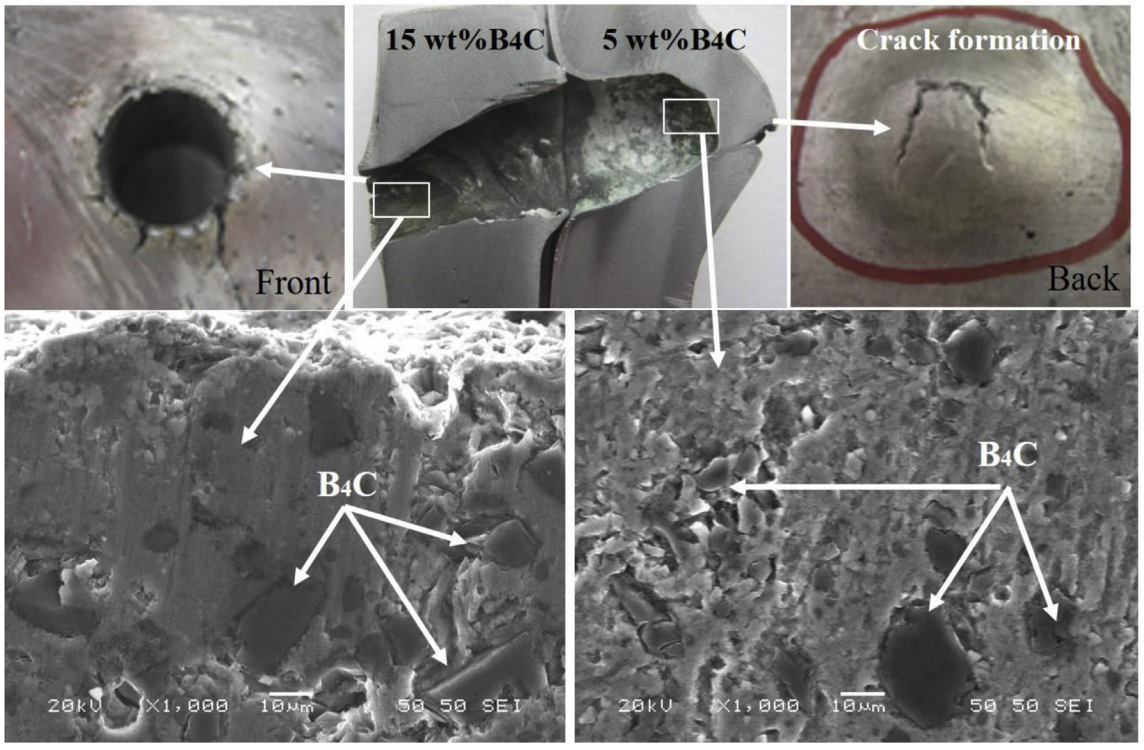

Fig. 13. Digital images of the front face, cross sectioning and back face of impacted armor. Bulging and small amount of crack formation on the back face. SEM images from penetration areas.

hot-rolled samples were studied. The effect of B_4C particle reinforcement in Al 6061 matrix on microstructure, mechanical and ballistic performance was investigated as a function of hot-extruded and hot-rolling production processes. The main results of this experimental investigation are summarized below:

- Relative density values above 98% were obtained in all B_4C particle-reinforced samples. The relative density of unreinforced Al 6061 specimens was measured as 99.26% and 99.62% for the hot-extrusion and hot-rolling processes, respectively. The density of the specimens reduced with increasing reinforcement particle ratio, and the porosity increased with particle weight fraction. The density of the specimens was significantly affected by the hot-extrusion process while the hot-rolling process did not have a remarkable effect on the density. However, the porosity of the specimens decreased after the hot-rolling process.
- Hardness values were increased with increasing B_4C particle reinforcement in a matrix structure and the highest hardness value was measured in the 20 wt% B_4C particle-reinforced Al 6061 hot-rolled composite specimen.
- The B_4C particle reinforcement improved the tensile strength and TRS of the hot-extruded and rolled composite specimens. The highest TRS was observed in 15 wt% B_4C particle-reinforced hot-extruded composite while the 5 wt% B_4C hot-rolled composite specimen exhibited the maximum tensile strength.
- The impact toughness of the composite specimens was decreased for both hot-extruded and rolled B_4C reinforced-composite specimens with increasing particle content. The highest impact energy was obtained in unreinforced Al 6061 specimens while the lowest impact energy was measured in 20 wt% B_4C particle-reinforced-composite specimens.
- Transgranular cracking was observed on the B_4C particles in the

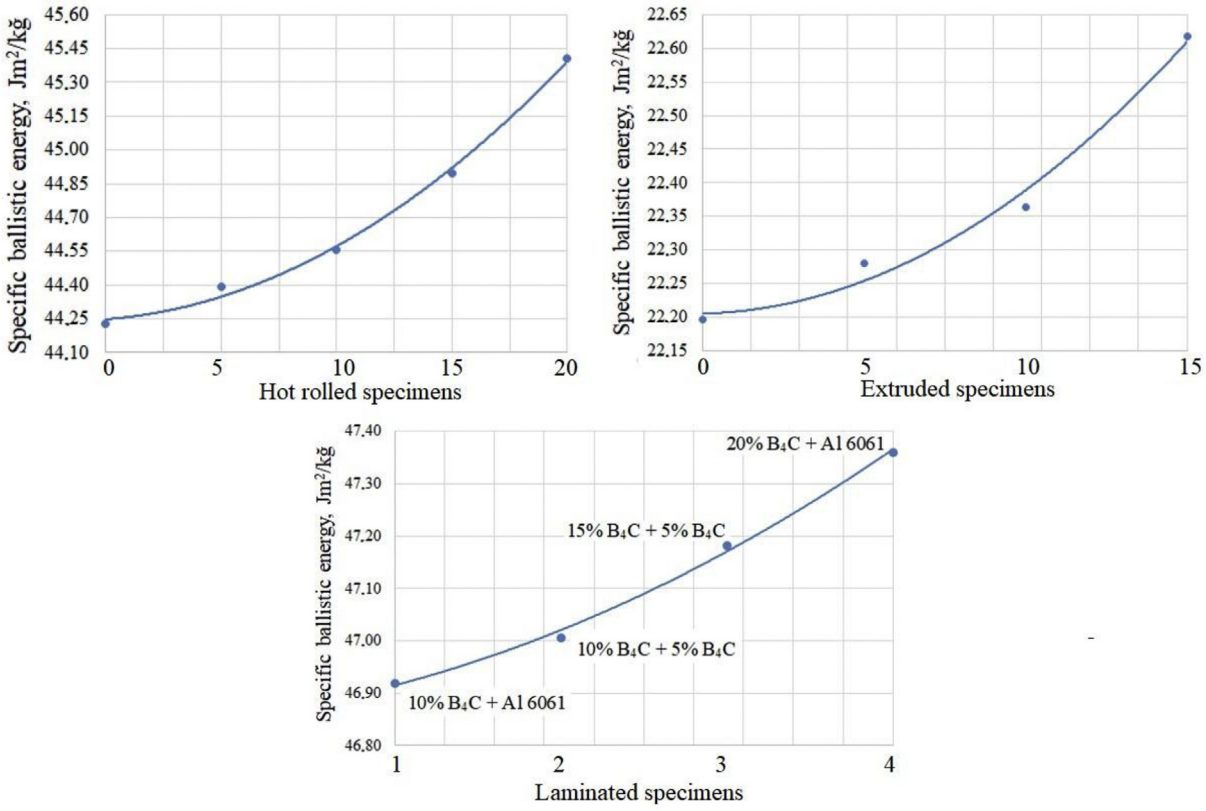

Fig. 14. The variation of specific ballistic energy of the specimens under study.

matrix after the deformation experiments.

- The 12.7 mm thick hot-rolled specimens were perforated in ballistic tests and exhibited ductile behavior. Radial cracks and spalling failure mechanism increased with increasing particle content in the matrix. The jacket of the projectile was peeled and remained in the hole for ballistic tests of all hot-rolled armor.
- The 25.4 mm thick hot-extruded specimens were also perforated in ballistic experiments and did not withstand the ballistic impact of the projectile. Petal formation with radial cracks was observed on the entrance and exit sides of the hole.
- The hot-rolled with two-layer composite specimens successfully absorbed the kinetic energy of the bullet with an acceptable depth of penetration. The first layer of the armor was penetrated and the second layer stopped the projectile. The best ballistic resistance was obtained in 5 wt% and 10 wt% B_4C layered composite armor.

Acknowledgments

The authors would like to acknowledge Gazi University Scientific Research Projects Coordination Unit for the financial support of this study 07/2015-09 and the Department of Materials and Metallurgy Engineering for the laboratory facilities. Special thanks go to the security general directorate criminal department for executing the ballistic tests.

References

[1] Karabulut Ş, Karakoç H, Çıtak R. Influence of B_4C particle reinforcement on mechanical and machining properties of Al6061/B_4C composites. Compos B Eng 2016;101:87–98.
[2] Karabulut Ş, Gökmen U, Çinici H. Study on the mechanical and drilling properties of AA7039 composites reinforced with Al_2O_3/B_4C/SiC particles. Compos B Eng 2016;93:43–55.
[3] Ibrahim MF, Ammar HR, Samuel AM, Soliman MS, Almajid A, Samuel FH. Mechanical properties and fracture of Al–15 vol.-% B_4C based metal matrix composites. Int J Cast Met Res 2014;27:7–14.
[4] Auradi V, Rajesh GL, Kori SA. Processing of B4C particulate reinforced 6061Aluminum matrix composites by melt stirring involving two-step addition. Procedia Mater Sci 2014;6:1068–76.
[5] Ibrahim MF, Ammar HR, Samuel AM, Soliman MS, Samuel FH. On the impact toughness of Al-15 vol.% B_4C metal matrix composites. Composer Part B 2015;79:83–94.
[6] Karamis MB, Tasdemirci A, Nair F. Failure and tribological behaviour of the AA5083 and AA6063 composites reinforced by SiC particles under ballistic impact. Composer Part A Appl Sci Manuf 2003;34:217–26.
[7] Karamis MB, Nair F, Tasdemirci A. Analyses of metallurgical behavior of Al-SiCp composites after ballistic impacts. Compos Struct 2004;64:219–26.
[8] Karamiş MB, Cerit AA, Nair F. Surface characteristics of projectiles after frictional interaction with metal matrix composites under ballistic condition. Wear 2006;261:738–45.
[9] Karamis MB, Nair F, Cerit AA. The metallurgical and deformation behaviours of laminar metal matrix composites after ballistic impact. J Mater Process Technol 2009;209:4880–9.
[10] Demir T, Übeyli M, Yildirim RO. Investigation on the ballistic impact behavior of various alloys against 7.62 mm armor piercing projectile. Mater Des 2008;29:2009–16.
[11] Holmen JK, Johnsen J, Jupp S, Hopperstad OS, Børvik T. Effects of heat treatment on the ballistic properties of AA6070 aluminium alloy. Int J Impact Eng 2013;57:119–33.
[12] Mondal C, Mishra B, Jena PK, Siva Kumar K, Bhat TB. Effect of heat treatment on the behavior of an AA7055 aluminum alloy during ballistic impact. Int J Impact Eng 2011;38:745–54.
[13] Zhou Z, Wu G, Jiang L, Li R, Xu Z. Analysis of morphology and microstructure of B4C/2024Al composites after 7.62mm ballistic impact. Mater Des 2014;63:658–63.
[14] Liu W, Chen Z, Cheng X, Wang Y, Amankwa AR, Xu J. Design and ballistic penetration of the ceramic composite armor. Compos B Eng 2016;84:33–40.
[15] Wadley HNG, O'Masta MR, Dharmasena KP, Compton BG, Gamble EA, Zok FW. Effect of core topology on projectile penetration in hybrid aluminum/alumina sandwich structures. Int J Impact Eng 2013;62:99–113.
[16] Garcia-Avila M, Portanova M, Rabiei A. Ballistic performance of composite metal foams. Compos Struct 2015;125:202–11. http://dx.doi.org/10.1016/j.compstruct.2015.01.031.
[17] McWilliams B, Yu J, Klier E, Yen C-F. Mechanical response of discontinuous ceramic fiber reinforced metal matrix composites under quasi-static and dynamic loadings. Mater Sci Eng, A 2014;590:21–9.
[18] Gilioli A, Manes A, Giglio M, Wierzbicki T. Predicting ballistic impact failure of aluminium 6061-T6 with the rate-independent Bao–Wierzbicki fracture model. Int J Impact Eng 2015;76:207–20.
[19] Manes A, Lumassi D, Giudici L, Giglio M. Thin-Walled Structures an experimental –

numerical investigation on aluminium tubes subjected to ballistic impact with soft core 7. 62 ball projectiles. Thin-Walled Struct 2013;73:68–80.
[20] Lee W, Lai C, Chiou S. Numerical study on perforation behavior of 6061-T6 aluminum matrix composite. J Mater Process Technol 2001;117:125–33.
[21] Aydin M, Apalak MK. Materials Science & Engineering A Experimental damage analysis of Al/SiC functionally graded sandwich plates under ballistic impact. Mater Sci Eng, A 2016;671:107–17.
[22] Jang S, Chung J, Seo S, Lee S, Lee Y, Lee S, Choi HJ. Enhancement of interfacial adhesion based on nanostructured alumina/aluminum laminates. Compos B Eng 2017;129:204–9.
[23] Clayton JD. Modeling effects of crystalline microstructure, energy storage mechanisms, and residual volume changes on penetration resistance of precipitate-hardened aluminum alloys. Compos B Eng 2009;40:443–50.
[24] Pavlovic A, Fragassa C, Disic A. Comparative numerical and experimental study of projectile impact on reinforced concrete. Compos B Eng 2017;108:122–30.
[25] Bresciani LM, Manes A, Ruggiero A, Iannitti G, Giglio M. Experimental tests and numerical modelling of ballistic impacts against Kevlar 29 plain-woven fabrics with an epoxy matrix: macro-homogeneous and Meso-heterogeneous approaches. Compos B Eng 2016;88:114–30.
[26] Bandaru AK, Ahmad S. Modeling of progressive damage for composites under ballistic impact. Compos B Eng 2016;93:75–87.
[27] Kędzierski P, Popławski A, Gieleta R, Morka A, Sławiński G. Experimental and numerical investigation of fabric impact behavior. Compos B Eng 2015;69:452–9.
[28] Wang JX, Zhou N. Experimental and numerical study of the ballistic performance of steel fibre-reinforced explosively welded targets impacted by a spherical fragment. Compos B Eng 2015;75:65–72.
[29] Zhou Y, Chen X. A numerical investigation into the influence of fabric construction on ballistic performance. Compos B Eng 2015;76:209–17.
[30] Ansari MM, Chakrabarti A, Iqbal MA. An experimental and finite element investigation of the ballistic performance of laminated GFRP composite target. Compos B Eng 2017;125:211–26.
[31] Chen X, Zhou Y, Wells G. Numerical and experimental investigations into ballistic performance of hybrid fabric panels. Compos B Eng 2014;58:35–42.
[32] Metal Powder Industries Federation: Standard test methods for metal powders and powder metallurgy products, New jersey. 1998.
[33] Metal Powder Industries Federation: standard test methods for metal powders and powder metallurgy products, Newjersey. 1998.
[34] NIJ 0101.06-U.S.. Department of Justice. Ballistic resistance of body armor NIJ standard 0101.06. 2008.
[35] Min S, Chen X, Chai Y, Lowe T. Effect of reinforcement continuity on the ballistic performance of composites reinforced with multiply plain weave fabric. Compos B Eng 2016;90:30–6.
[36] Balaganesan G, Chandra Khan V. Energy absorption of repaired composite laminates subjected to impact loading. Compos B Eng 2016;98:39–48.
[37] Groover MP. Fundamentals of modern manufacturing: materials processes, and systems. 5 John Wiley & Sons; 2007.
[38] Canakci A. Microstructure and abrasive wear behaviour of B4C particle reinforced 2014 Al matrix composites. J Mater Sci 2011;46:2805–13.
[39] Chen HS, Wang WX, Li YL, Zhang P, Nie HH, Wu QC. The design, microstructure and tensile properties of B_4C particulate reinforced 6061 Al neutron absorber composites. J Alloy Comp 2015;632:23–9.
[40] Wang B, Chou S. The behaviour of laminated composite plates as armour. J Mater Process Technol 1997;68:279–87.
[41] Zaera R, Sánchez-Sáez S, Pérez-Castellanos JL, Navarro C. Modelling of the adhesive layer in mixed ceramic/metal armours subjected to impact. Composer Part A Appl Sci Manuf 2000;31:823–33.
[42] Mapelli C, Manes A, Giglio M, Mombelli D, Baldizzone C. Microstructural investigation on an Al 6061 T6 alloy subjected to ballistic impact. Procedia Eng 2011;10:3447–52.
[43] Tan VBC, Tay TE, Teo WK. Strengthening fabric armour with silica colloidal suspensions. Int J Solid Struct 2005;42:1561–76.